Electronic Supplementary Information for

Electrically Powered Artificial Black Body for Low-voltage High-speed Interfacial Evaporation

Fenghua Liu [a], Hongru Pang [b], Yunjiao Gu[a], Yuesheng Ning [b], Robert Bradley[c,d,e], Binyuan Zhao[b]* and Weiping Wu[a]*

[a] *State Key Laboratory of High Field Laser Physics, Shanghai Institute of Optics and Fine Mechanics, Chinese Academy of Sciences, Shanghai, 201800, China; Key Laboratory of Materials for High Power Laser, Shanghai Institute of Optics and Fine Mechanics, Chinese Academy of Sciences, Shanghai, 201800, China; Laboratory of Thin Film Optics, Shanghai Institute of Optics and Fine Mechanics, Chinese Academy of Sciences, Shanghai 201800, China; Email: wuwp@siom.ac.cn*

[b] *State Key Laboratory of Metal Matrix Composites, School of Materials Science and Engineering, Shanghai Jiao Tong University, Shanghai, 200240, China; Email: byzhao@sjtu.edu.cn*

[c] *Department of Materials, University of Oxford, 16 Parks Road, Oxford, OX1 3PH, United Kingdom*

[d] *MatSurf Technology Ltd., The Old Stables Marion Lodge, Little Salkeld, Penrith Cumbria, CA10 1NW, United Kingdom*

[e] *School of Energy Resources, University of Wyoming, Laramie, WY, 82071, USA*

∗ Corresponding authors. Email: wuwp@siom.ac.cn (W. Wu), byzhao@sjtu.edu.cn (B. Zhao)

Contents

Figure S1 The schematic diagram of the preparation process of MPC.

Figure S2 The Fourier-transform infrared spectroscopy (FTIR) of the MPC.

Figure S3 The X-ray spectrum (XPS) of the MPC.

Figure S4 The Raman spectroscopy of the MPC.

Figure S5 The photo of the MPC/cloth-F device for vapor generation via Joule heat.

Figure S6 The evaporation rate with different devices in 1 L sea water.

Figure S7 The photos of the CrNi wire evaporator and the microstructures of the hydrophilic cloth.

Figure S8 The comparison for vapor generation of the MPC and CrNi wire which were directly used as heating bodies, and the cloth was used as a water absorption and evaporation layer.

Figure S9 The curve of the input power as a function of voltage.

Figure S10 The influence of wind speed on interfacial evaporation under low energy input.

Figure S11 The effect of evaporation rate for applying the wind with speed of 3 m s^{-1}.

Figure S12 The photograph of the MPC after evaporation of running 10 hours.

Table S1 The change of salt ion concentration before and after the Joule thermal interfacial evaporation.

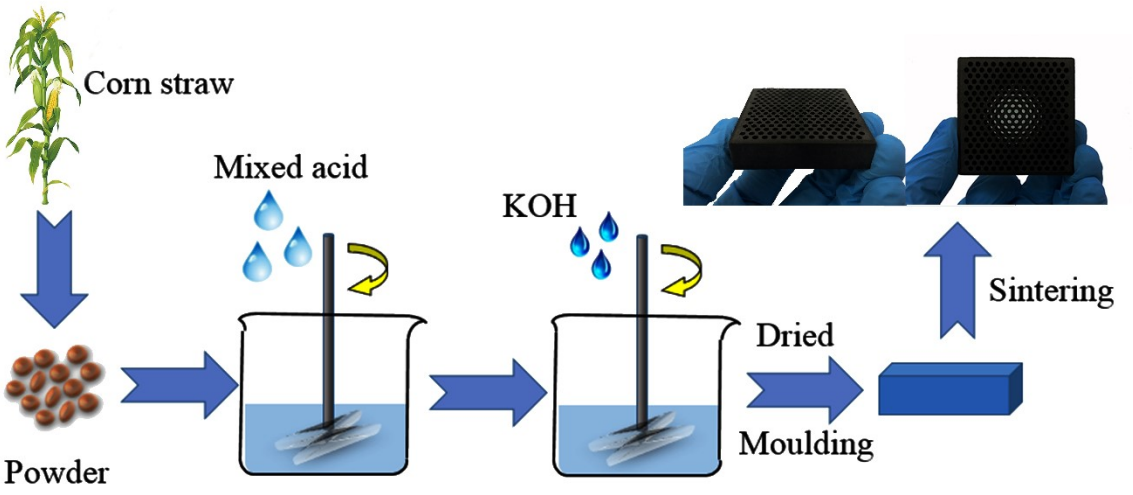

Figure S1 The schematic diagram of the preparation process of MPC. This artificial black body can be obtained by compression molding and activation from biomass. It has a rich pore structure and a realitive high specific surface area, which can achieve a larger specific surface area per uint volume and is suitable for interfacial evaporation via solar thermal or Joule heating. It is an excellent carrier to realize high speed vapor generation and save space.

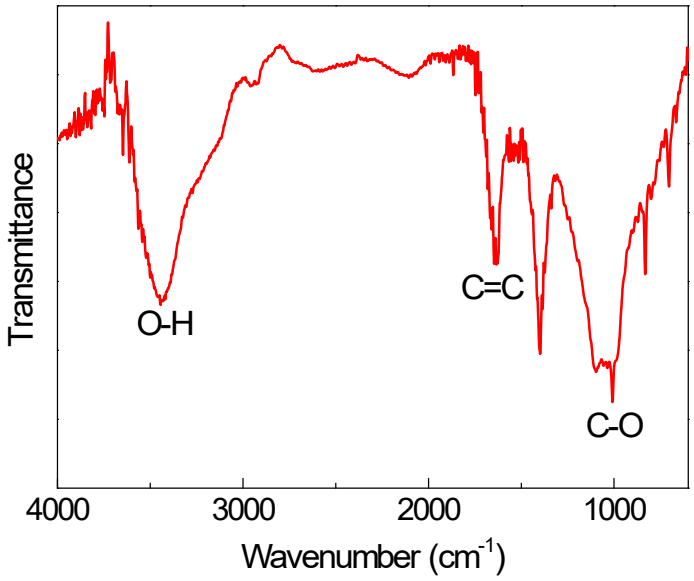

Figure S2 The Fourier-transform infrared spectroscopy (FTIR) of the MPC. It can be found from the figure that the MPC contains polar functional groups, such as C=C(1631 cm^{-1}), C-O (1109 cm^{-1}) and O-H (3419 cm^{-1}). Due to the existence of these polar functional groups, the MPC exhibits a certain degree of hydrophilicity. These features will facilitate the conduction of water.

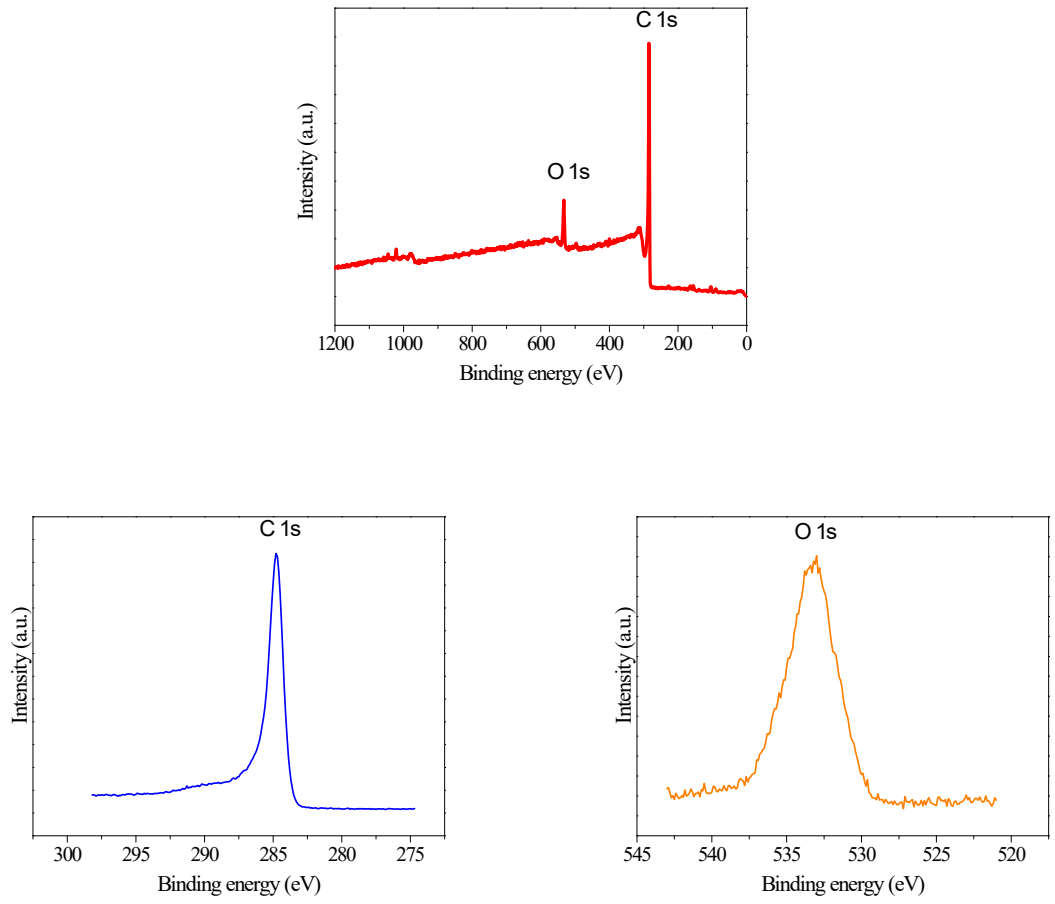

Figure S3 The X-ray spectrum (XPS) of the MPC. The surface chemical compositions of MPC was identified by X-ray photoelectron spectroscopy (XPS) and strong C 1s (284.7 eV) and O 1s (533 eV) peaks were observed. The surface chemical element composition derived from the XPS results showing that the amount of carbon (C) is ≈91.1%, oxygen (O) is about 8.8%.

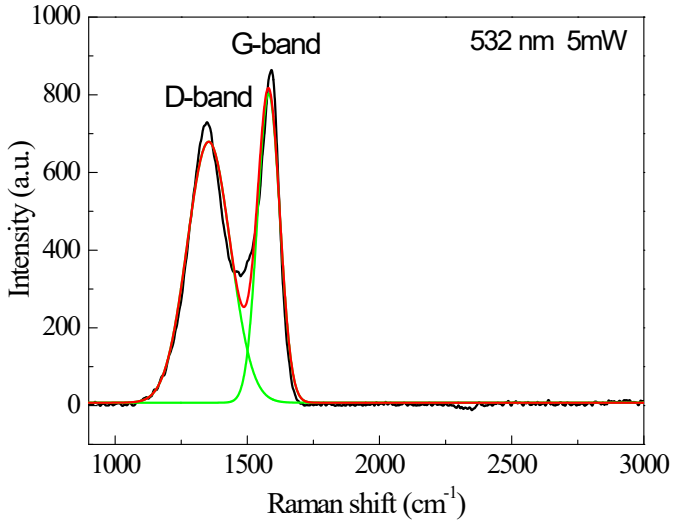

Figure S4 The Raman spectroscopy of the MPC. In Raman spectroscopy, the intensity ratio of peak D to peak G (I_D/I_G) represents the degree of graphitization of carbon materials. The lower of the ratio, the degree of graphitization is higher, and the defects are fewer. It can be seen from the figure that the intensity ratio of the fitted peak D to the peak G is about 1.45. This shows that the MPC has a certain degree of graphitization.

Figure S5 The photo of the MPC/cloth-F device for vapor generation via Joule heat. During the experiment, the DC power supply provides Joule heat, and the resistance of the MPC is suitable for obtaining higher heat under lower voltages. The heat is relatively evenly distributed in the bulk material MPC. Because of the rich pore structure and high specific surface area of MPC, the interfacial evaporation of bulk materials is formed and the effect is excellent.

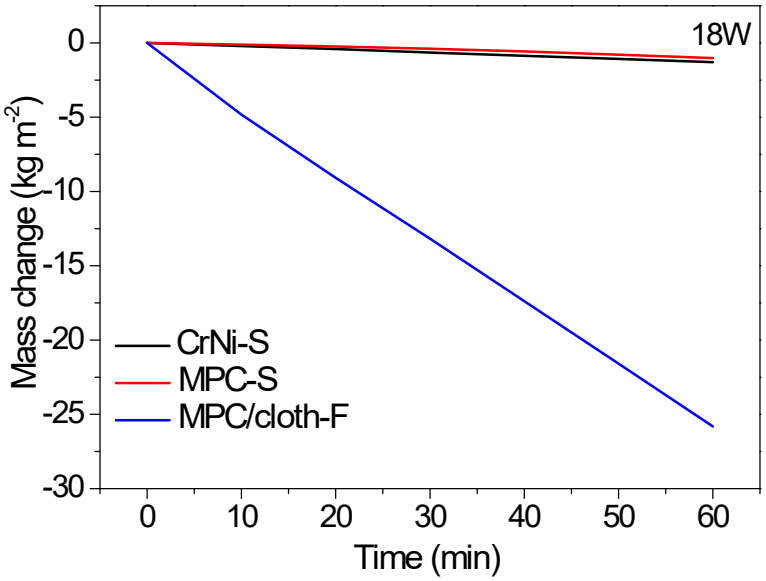

Figure S6 The evaporation rate with different devices in 1 L sea water. Since there is no nanoporous structure and high specific surface area, traditional Joule heat materials such as CrNi wire, need to heat the whole bulk water to realize the stable evaporation. The process of heating the salt water as a whole consumes a lot of heat, resulting in a low evaporation rate. In addition, CrNi wire is generally immersed in water, and the preheating period and the later period are directly affected by the volume of the whole bulk water. The energy consumption will be very high when the treated water increases. When the amount of water to be treated is large, the MPC immersed in water exhibit a similar effect with the CrNi wire. When the input power is 18 W, the water volume is 1000 ml, the evaporation rate of CrNi-S and MPC-S reached 1.02 kg m^{-2} h^{-1} and 1.3 kg m^{-2} h^{-1} during the first hour, respectively. While the water generation rate of the MPC/cloth-F designed as a floating structure reached 25.8 kg m^{-2} h^{-1}.

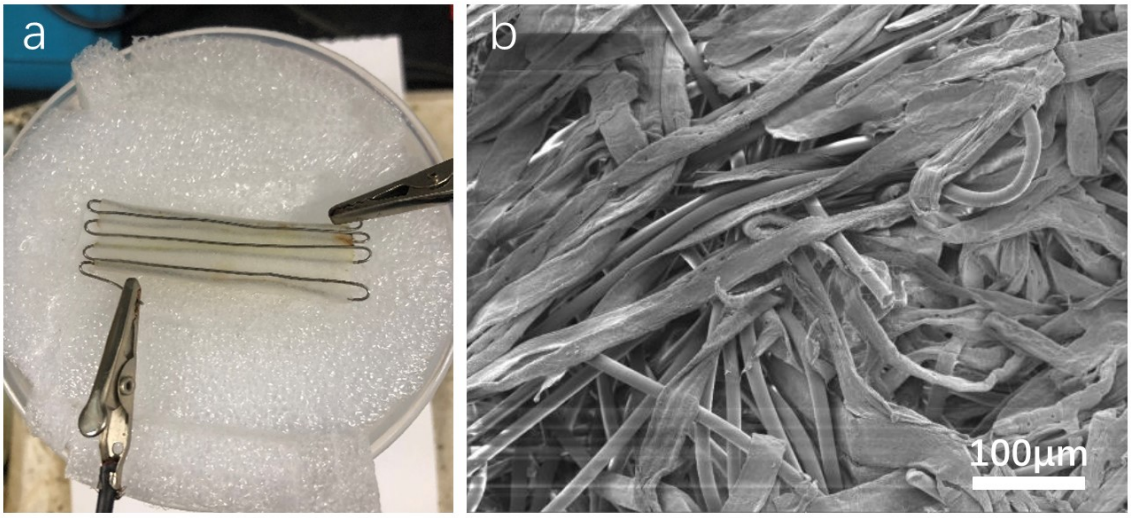

Figure S7 The photos of the CrNi wire evaporator and the microstructures of the hydrophilic cloth. (a) The photo of the CrNi wire crapped on the surface of the hydrophilic cloth for vapor generation with Joule heat. (b) The SEM photograph of the hydrophilic cloth. The strategy of covering the hydrophilic cloth with CrNi wire can also achieve a certain Joule heating interfacial evaporation. The CrNi wire can form a thermal field and conduct heat to the fiber cloth. This design also uses the idea of insulated floating structure. The fiber cloth has a rich specific surface area and nano/micro structure, providing a large number of interfaces for water evaporation.

In order to pursue the objectivity of the comparison, several adjustments have been made in the experiment design. The resistance value and surface area of the MPC and CrNi wire used in the manuscript are roughly equivalent. The size of the CrNi wire is Φ 0.4×20 cm. The external dimension of the MPC is 5×1×0.5 cm, and there are 44 macroscopic channels with a diameter of 0.2 cm. The CrNi wire and MPC have the roughly equivalent macroscopic surface area to ensure the same conditions in the water heat exchange area.

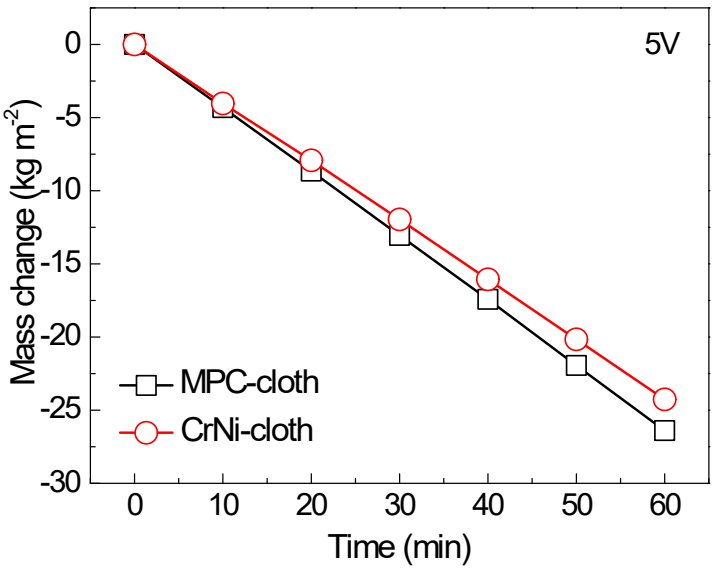

Figure S8 The comparison for vapor generation of the MPC and CrNi wire which were directly used as heating bodies, and the cloth was used as a water absorption and evaporation layer. The resistance of MPC and CrNi wire is roughly the same. Under the same voltage (5 V), the evaporation rate of these two devices combined with cloth are also relatively close. Among them, the evaporation rate of MPC is higher, which is mainly because MPC has certain advantages in comprehensive pore structure and heat control.

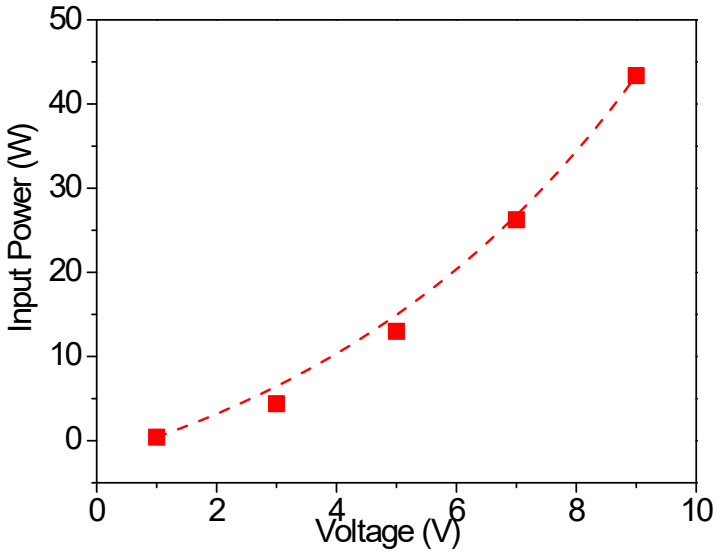

Figure S9 The curve of the input power as a function of voltage. The relationship between input power and voltage obviously conforms to the law of $P=U^2/R$. At the same time, comparing it with the curve of evaporation rate to voltage, it is not difficult to find that the relationship between evaporation rate and input power is linear.

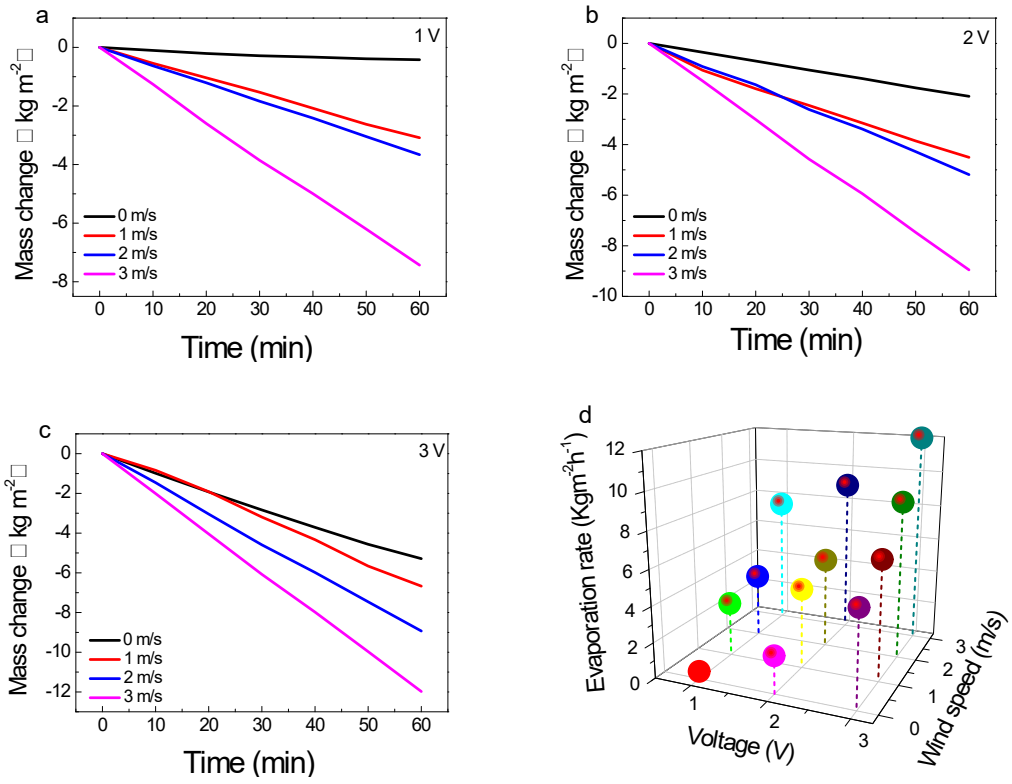

Figure S10 The influence of wind speed on interfacial evaporation under low energy input. (a) The voltage of 1 V, (b) The voltage of 2 V, (c) The voltage of 3 V, (d) The visual map of the combined effects of input voltage and windspeed on interfacial evaporation. In the experiments of our manuscript, wind-promoting evaporation only happened when the input voltage is low (1-3 V). With the enhanced wind speed (1-3 m s^{-1}), the evaporation rate gradually increases.

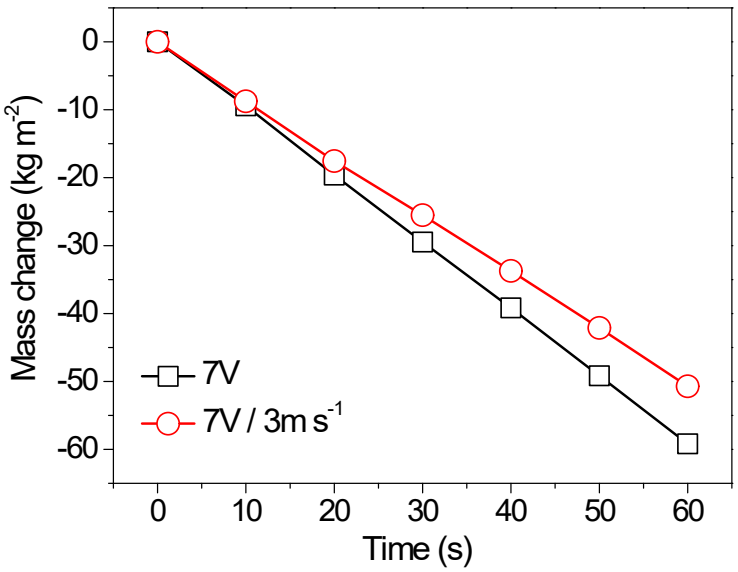

Figure S11 The effect of evaporation rate for applying the wind with speed of 3 m s^{-1}. At relatively high voltage, that is, when the input power is high, the effect of wind does not promote evaporation, but reduces the evaporation rate. This is because when the heat is relatively high, the evaporation performance is realized by heat energy, and the air convection in the upper part of the evaporation layer is significantly enhanced when the wind is introduced. Finally, the heat is lost through forced convection, which affects the evaporation efficiency.

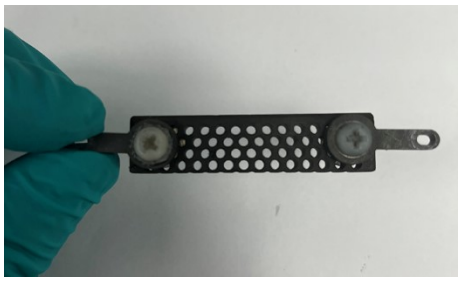

Figure S12 The photograph of the MPC after evaporation of running 10 hours. For the carrier of interfacial evaporation, the corrosion resistance in salt water is indeed a very important indicator. This electrically powered artificial black body is mainly composed of C and O elements (Figure S2, S3), which is an almost all-carbon porous material. Carbon materials with porous and conductive properties are generally inert to the environment, and therefore suitable for interfacial evaporation under electric fields. We also have designed the corrosion resistance of the device. Graphite connection was used in the connection part with MPC, especially in the position where it may come into contact with salt water, so as to ensure the environmental inertness of the whole device. The content of metals and other elements that are prone to electrochemical reactions in the raw materials is very small, and no obvious corrosion will occur even under the action of long-term electric heating.

Table S1 The change of salt ion concentration before and after the Joule thermal interfacial evaporation.

Ions concentration / mg L^{-1}	Na^{+}	Mg^{2+}	K^{+}	Ca^{2+}
Original	11210	8102	1127	9951
After desalination	7.8	5.6	9.1	4.3